

Stretchable optical diffraction grating from poly(acrylic acid)/polyethylene oxide stereocomplex

Jinghan He,[†] Andre Kovach,[‡] Yunxiang Wang,[§] Wei Wu,[§] Andrea M. Armani*,^{†,‡,§}

[†]Department of Chemistry, University of Southern California, Los Angeles, California 90089, United States

[‡]Mork Family Department of Chemical Engineering, University of Southern California, Los Angeles, California 90089, United States

[§]Ming Hsieh Department of Electrical and Computer Engineering, University of Southern California, Los Angeles, California 90089, United States

ABSTRACT: Optical gratings are a key component in many spectroscopy, communications, and imaging systems. While initially static elements, advances in optical materials have enabled dynamically tunable gratings to be designed. One common tuning strategy is relying on mechanical deformation of the grating pitch to modify the diffraction pattern. To date, most mechanically adaptive optical gratings consist of a hybrid system where rigid moieties are patterned on an elastomeric substrate. In the present work, we demonstrate an all-polymer tunable grating that is fabricated using replica molding from the poly(acrylic acid) (PAA)/polyethylene oxide (PEO) polymer stereocomplex. PAA/PEO pristine films exhibit excellent optical transmittance at or above 80% from 500 nm to 1400 nm and stretchability over 800% strain. The experimental studies on the changes of diffraction mode distances with respect to the applied strains agree well with the finite-difference time-domain (FDTD) theoretical modeling.

KEYWORDS: *diffraction grating, adaptive tuning, polymer complexes, optical materials,*

INTRODUCTION

Optomechanical systems are found throughout science and engineering, forming the foundation of microscopes, telescopes, and spectroscopy instrumentation as well as communication networks. Typically comprised of a complex array of lenses, gratings, and mirrors, these systems have been transformed from static to dynamically adaptable arrays through synergistic advances in materials chemistry and fabrication. While initial efforts focused on flexible mirrors for image correction in atmospheric science, the broader field of tunable or deformable optics has touched nearly all technical areas. One cross-cutting optical element is the diffraction grating.

Diffraction gratings are optical elements with a precisely defined periodic structure that can split or diffract an incident beam into a series of precisely spaced output beams.¹ Gratings can be designed to operate as either a transmissive or reflective structure, and the spacing of the diffracted beams is dependent on the incident angle, operating wavelength, grating distance, and refractive index. Given the flexibility of design and ability to separate or spread optical wavelengths, diffraction gratings are used in numerous applications, including integrated optics, spectroscopy, and telecommunications.²⁻¹² Given the broad utility, the development of a reversible adaptive diffraction grating could have a broad impact.

Because the diffraction performance is dependent on the geometric and optical properties of the grating, changing any of the metrics will result in a tunable element. Electrical and thermal tuning of conventional optical materials have both been demonstrated successfully, but an emerging strategy is based on strain or mechanical deformation of polymeric components. Unlike conventional crystalline materials, some polymers can exhibit large, reversible elastic properties.¹³⁻¹⁶ Therefore, by applying tensile strain, any patterned optical structures will be deformed, leading to the tuning of the diffraction properties.¹⁷⁻²⁸

One advantage of using a polymer to fabricate a device is its compatibility with transfer or replica molding, where micro/nano patterns fabricated using nanolithography or nanoimprint lithography are transferred to the soft substrate, creating a stretchable device. This fabrication approach greatly simplifies the fabrication process, reducing the overall fabrication cost per part and accelerating manufacturing. However, independent of the approach used, the reversibility of the deformation, amount of deformation, and operating wavelength are all governed by the specific polymer used.

In this work, we use replica molding to fabricate a deformable diffraction grating based on the polymer stereocomplex poly(acrylic acid) (PAA)/polyethylene oxide (PEO). Due to the broad optical transparency and high elasticity, the grating operates from the visible through the near-IR, and the diffraction pattern was reversibly changed by applying mechanical strain to the grating (Figure 1).

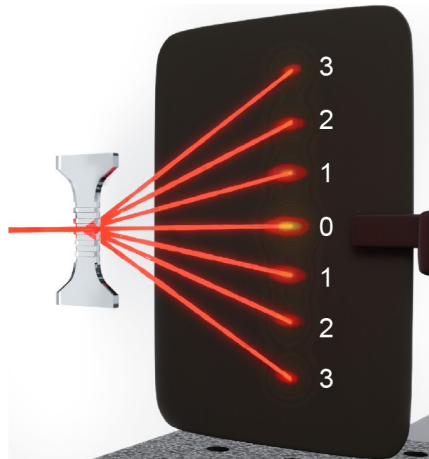


Figure 1. Illustration of the grating structure and generated diffraction pattern. The mode orders (0^{th} , 1^{st} , 2^{nd} , and 3^{rd}) are indicated.

RESULTS AND DISCUSSION

Finite-difference time-domain (FDTD) simulations. The first three diffraction modes of the PAA/PEO polymer gratings undergoing deformation were simulated with FDTD methods. The

starting grating geometry was determined from scanning electron microscopy images of the experimental structure, and subsequent geometries were based on the elasticity of the material. Both visible (633 nm) and near-IR (1300 nm) incident wavelengths were studied. Figure 2 summarizes the FDTD simulation results. The results are plotted as both the separation distance between adjacent modes and the separation from the 0th mode.

For both 633 and 1064 nm, as the strain on the polymer grating gradually increases, the grating pitch increases, resulting in decreased diffraction angles and decreased diffraction mode distances. While the separation distances scale with wavelength, as expected, the general trend and dependence on strain is similar at both wavelengths.

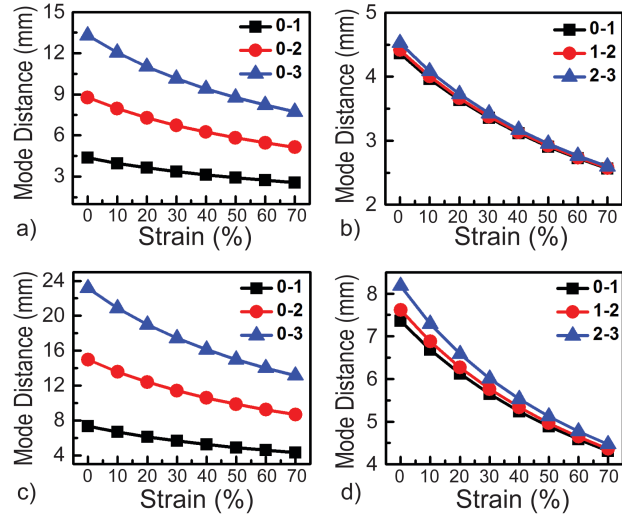


Figure 2. FDTD simulations of the first three diffraction mode separation distances of the PAA/PEO stereocomplex grating at different strain values and incident wavelengths. a) At incident wavelength of 633 nm, the separation from the 0th mode is analyzed. b) At incident wavelength of 633 nm, the separation from adjacent modes is analyzed. The mode spacing slightly increases. c) At incident wavelength of 1064 nm, the separation from the 0th mode is analyzed. d) At incident wavelength of 1064 nm, the separation from adjacent modes is analyzed.

The mode spacing slightly increases.

PAA/PEO characterization. To prepare a uniform, self-supporting polymer sample for optical and mechanical characterization, the PAA/PEO polymer stereocomplex pellets were first formed using procedures similar to previous works.^{16,29} The molar ratio of COOH groups in PAA over oxygen segment in PEO is ideally 1:1 to facilitate the formation of the intermolecular hydrogen bonds, resulting into a uniform and robust network. To create a continuous and uniform film, the pellets were compressed between a pair of polytetrafluoroethylene (PTFE) sheets (Figure 3). Additional details on the pellet formation and film fabrication are included in the Methods Section.

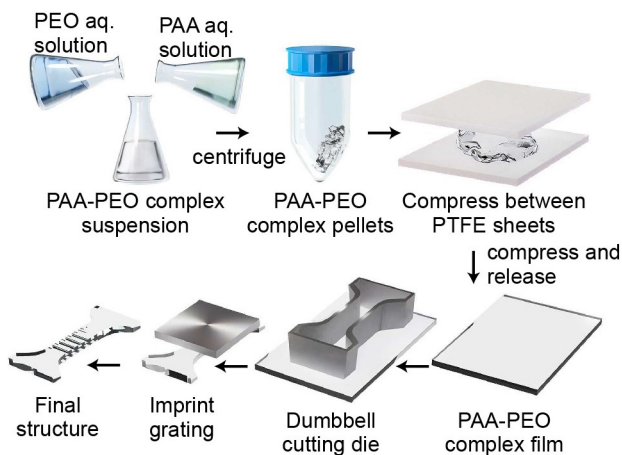


Figure 3. Outline of the material synthesis and the fabrication of the PAA/PEO polymer stereocomplex diffraction grating.

The UV-Vis transmittance spectrum of the PAA/PEO sample is shown in Figure 4. As can be seen from the spectrum, this polymer is ideally suited for optical applications as the transmission is at or above 80% from 500 to 1400 nm. To explore this entire range, we focused on 633 nm and 1064 nm. At this pair of wavelengths, the transmission is 82% and 85%, respectively.

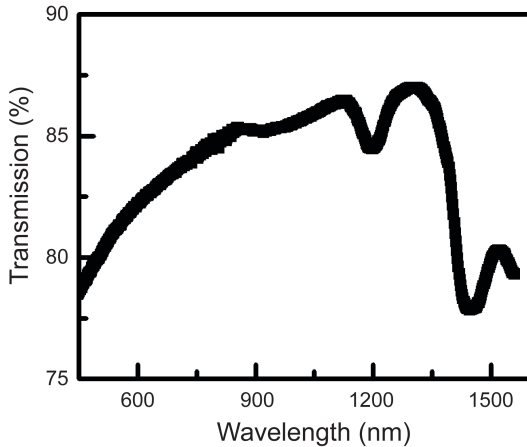


Figure 4. UV-Vis absorption spectrum of PAA/PEO stereocomplex film.

The PAA/PEO film was cut into a dumbbell shape using an ISO standard die cutter. The sample was mounted on an Instron tensile test instrument using a pair of pneumatic clamps, and the mechanical response to tensile strain was analyzed. The stress-strain curve of the PAA/PEO sample is shown in Figure S3. As seen, the elongation at the break is above 800% strain, demonstrating significant elasticity of the film. However, there is also permanent deformation at these high strain values. To achieve reversibility with minimal sample damage, it was necessary to apply less than 80% strain. As can be seen in the cyclic testing of the polymer sample (Figure 5), all five measurements exhibit a noticeable hysteretic behavior with significant energy loss after the first cycle. This is expected because of the dynamic hydrogen bonds in the PAA/PEO stereocomplex which can lead to strain accumulation and deformation of the sample. (Figure 5, inset). It should be noted that all five cycles were performed iteratively without any recovery time in between the measurements. Given sufficient time (~1d), the material response recovered (Figure S4).

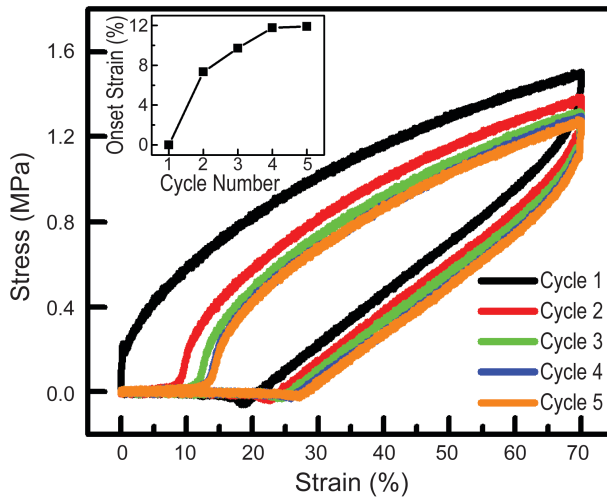


Figure 5. Five loading-unloading tensile test cycles of the PAA/PEO polymer film. Inset: Onset strain in each hysteresis loop cycle.

Grating fabrication and characterization. The stretchable transmission grating was fabricated from a Si master structure using replica molding (Figure 6a). When performing the molding step, the grating structure (Figure 6b) was oriented perpendicular to the vertical axis of the die cut-out. The dumbbell die ensured that force would be uniformly applied across the grating during deformation according to ISO standards. As a result, the pitch and periodicity of the grating would increase predictably. As shown in Figure 6, the molding process was able to accurately replicate the nano and microscale features over a large area.

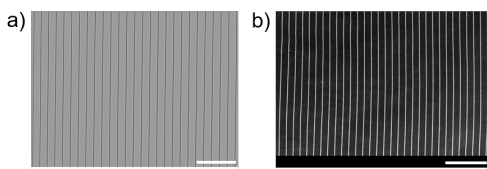


Figure 6. SEM images of a) Silicon master grating and b) the PAA/PEO polymer grating. Scale bar is 50 μm .

To characterize the optical performance of the stretchable grating an optical test bench was integrated into the Instron (Figure 7). The diffraction at both 633 nm and 1064 nm was

characterized to explore both the visible and near-IR wavelength ranges (Figure S5). The laser beam spot was focused on the grating with a collimator and a lens. A beam splitter, a receiving screen, and a camera were used to receive and detect the diffraction patterns. Data was taken at discrete strain values (steady state strain values).

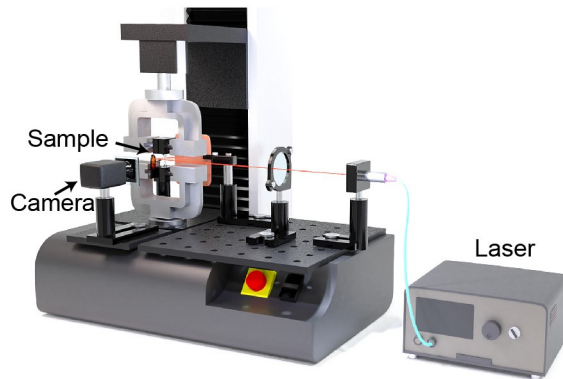


Figure 7. Testing setup for the polymer grating consists of a 633 nm or 1064 nm laser, a universal tensile test machine (Instron) to apply continuous strains, a beam splitter, a receiving screen, and a camera to capture diffraction pattern images.

A representative series of images from both wavelengths is shown in Figure 8. An initial inspection of the data reveals that the initial mode separations at 1064 nm are larger than 633 nm separations. At both wavelengths, the separation distance decreases with increasing strain, and then it recovers when the strain is removed. These results all agree with the FDTD modeling.

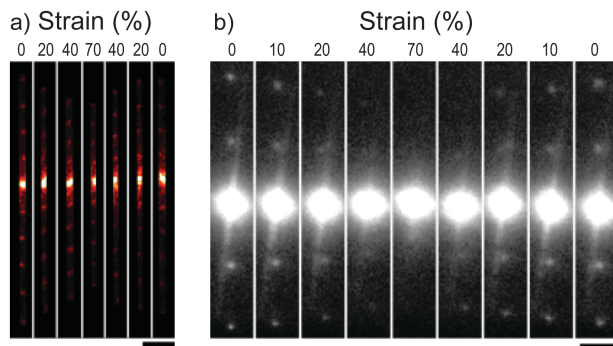


Figure 8. The diffraction patterns generated at a) 633 nm and b) 1064 nm during one stretching-and-relaxing cycle are shown. The cycle started at 0% strain, increased to a maximum of 70% strain, and returned to 0% strain. Scale bar is 5 mm.

To analyze the data more rigorously and quantitatively, the mode separation distances were measured on the receiving screen. The diffraction patterns with respect to strains at 633 nm for all five cycles are depicted in Figure 9. As the grating was stretched from 0% to 70% strain, the diffraction mode distances of 0^{th} - 1^{st} , 0^{th} - 2^{nd} and 0^{th} - 3^{rd} changed by \sim 1.5 mm, \sim 3 mm, and \sim 4.5 mm, respectively. While the general trend of experimental and theoretical results (Figure 2a,b) is in a good agreement, there are a couple of interesting points to note. First, in Figure 9a,c,e, for the second stretching cycle, the first strain step (0% to 10%) actually increases the mode separation. This is the opposite behavior expected. Additionally, the mode separation does not fully return to the initial starting point after being strained. However, it is important to recall the mechanical test results presented in Figure 5 in which the second cycle did not exactly replicate the mechanical response of the first cycle. Therefore, most likely, both results are due to an accumulated deformation of the grating which occur over the strains studied.

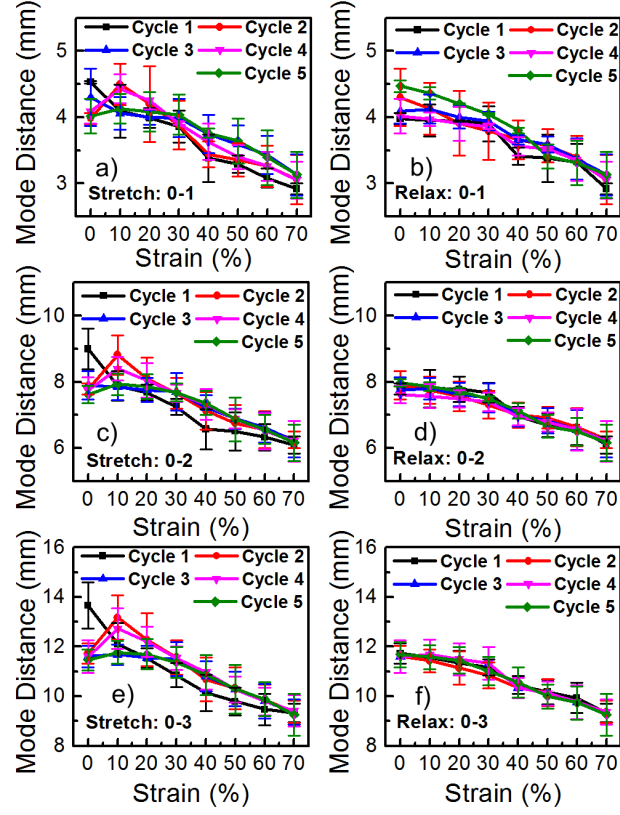


Figure 9. Measurements of strain-induced changes in the spacing between diffracted modes at 633 nm. Measurements are with respect to the 0th mode. a) 0th-1st mode, stretching; b) 0th-1st mode, relaxing; c) 0th-2nd mode, stretching; d) 0th-2nd mode, relaxing; e) 0th-3rd mode, stretching; f) 0th-3rd mode, relaxing.

Figure 10 summarizes the mode distances measured at 1064 nm. Due to the significantly increased mode spacing at 1064 nm, the imaging screen is only able to capture up to second order diffraction modes from 0 % to 20% strains (Figure 8b).

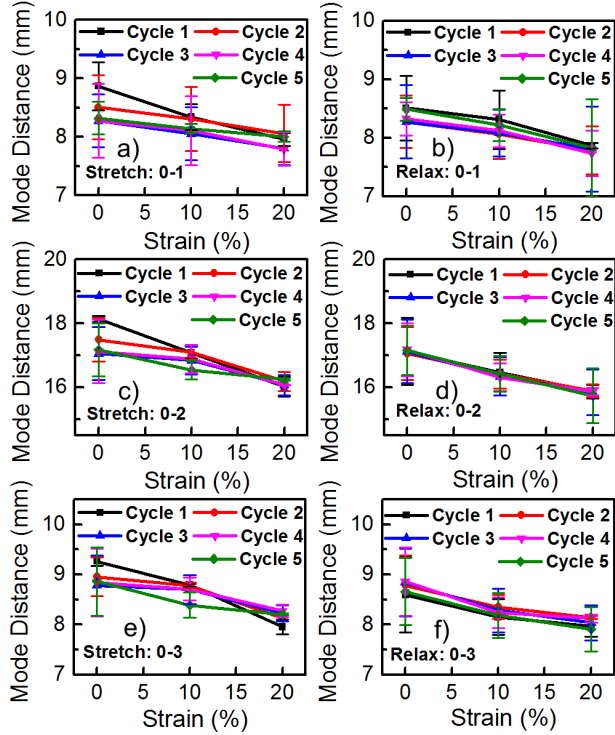


Figure 10. Measurements of strain-induced changes in the spacing between diffracted modes at 1064 nm. Measurements are with respect to the 0th mode. a) 0th-1st mode, stretching; b) 0th-1st mode, relaxing; c) 0th-2nd mode, stretching; d) 0th-2nd mode, relaxing; e) 1st-2nd mode, stretching; f) 1st-2nd mode, relaxing.

As the grating was stretched from 0% to 20% strain, the diffraction mode distances of 0th-1st and 0th-2nd changed by \sim 0.5 mm and \sim 1.5 mm, respectively. These results also correspond well with the theoretical simulations in Figure 2c,d. Similar to the findings at 633 nm, the accumulated strains in the polymer during cycling also limited the ability of the grating to fully recover. This was particularly pronounced during the first cycle.

CONCLUSIONS

In summary, we have proposed and demonstrated a deformable polymer grating using a combination of nanoimprint and soft lithography. The PAA/PEO polymer stereocomplex has high

optical transparency throughout most of the visible and near-IR wavelength ranges as well as a high percent elongation before failure (800%). Additionally, due to the intermolecular dynamic hydrogen bonds in the PAA/PEO stereocomplex, the polymer can be reversibly loaded and unloaded at lower strains. This combination of features makes it ideally suited for a deformable optical element. Using replica molding, the micro-scale structures of the Si grating template are accurately transferred to the PAA/PEO polymer stereocomplex, creating the deformable grating. In general, at both 633 nm and 1064 nm, the diffraction mode distances agreed with the theoretical simulations. This system opens a novel pathway towards adaptive and tunable optical gratings, which could have a wide range of applications, such as tunable spectroscopy, sensing and optical filters. The future studies may lie in the optimization of the material designs, integration of optically active components and fabrication of more complex optical elements.

METHODS

Polymer film preparations. PAA ($M_w = 240\,000$, BeanTown Chemical) and PEO ($M_w = 1\,000\,000$, Alfa Aesar) were used as received. The preparation protocol of PAA/PEO polymer stereocomplex was similar to previous works with a few differences noted here.^{16,29} Typically, PEO aqueous solution (2.9 mg/mL, 50 mL, pH 2.8) and PAA aqueous solution (1.8 mg/mL, 50 mL, pH 2.8) were prepared in two separate beakers. Then, two aqueous solutions were slowly mixed into a third beaker via a syringe pump at a rate of 5 mL/min, precipitating PAA/PEO pellets which were further collected via centrifugation (7800 relative centrifugal force, overnight).

Fabrication of stretchable grating. To form a uniform polymer film, PAA/PEO complex pellets were placed between two PTFE sheets and compressed by Al blocks (~5 kPa) for one day before peeling off. A dumbbell-shaped film cutting die (Model Standard ISO 37-4) was used as the stamp to shape PAA/PEO film into a standard tensile specimen. Then, the hydrophobic Si master grating

(preparation procedure in SI) was placed upside down on top of the stamped polymer film to perform the replica molding (~ 5 kPa for 30 min at room temperature) of PAA/PEO grating. Finally, the hydrophobic Si master grating was peeled off to obtain the polymer grating. For initial inspection, a polymer grating was coated with platinum using sputter coating and imagined using scanning electron microscopy (FEI Nova NanoSEM).

Material characterization. To apply mechanical stretches on the PAA/PEO polymer film, tensile tests (including the cyclic loading-unloading tests) were implemented on a universal tensile testing machine with pneumatic clamps (Instron 3340, stretching rate 50% strain/min) under ambient conditions. UV–Vis transmittance spectrum of a PAA/PEO polymer film was recorded by a LAMBDA 950 UV/Vis Spectrophotometer (PerkinElmer).

Optical characterization methods. To experimentally study how the PAA/PEO polymer grating is adaptively responded to the external mechanical strains, the strains on the polymer grating specimen was precisely controlled via the Instron universal tensile test instrument (Instron 3340, stretching rate 50% strain/min). There are several optical components well aligned around the Instron shown in Figure 7. The incident light was provided either from 633 or 1064 nm laser, the best two wavelengths in terms of the quality of the diffraction patterns under the camera (Figure S5). The laser beam spot was focused on the grating with a collimator and a lens. A beam splitter, a receiving screen and a camera were used to receive the diffraction patterns.

Simulations. The theoretical diffraction mode distances of the polymer grating were modeled using the finite-difference time-domain (FDTD; Lumerical Solutions, Inc.) method. A single cell was modeled using periodic boundary conditions in the in-plane dimensions and perfectly matched layers in the out-of-plane dimensions. PAA/PEO polymer stereocomplex is considered as the Cauchy model with Cauchy parameters $A = 1.45$, $B = 0.01$ and $C = 0$. The initial grating sizes,

including the pitch, linewidth, and height of the polymer grating, were set to 10 μm , 500 nm and 1 μm , respectively. The simulation single cell of the polymer grating is considered as a steady state where the dimension of the single cell is rearranged accordingly with the applied strain; therefore, when modeling the polymer grating at each strain, each single cell dimension is redefined with respect to the corresponding strain.

SUPPORTING INFORMATION

The supporting information is available free of charge on the ACS Publication website.

AUTHOR INFORMATION

Corresponding Author

*E-mail: armani@usc.edu

Author Contributions.

The manuscript was written through contributions of all authors. J. H. prepared all samples, performed material analysis, conducted optical characterizations, and analyzed data. A. K. designed the optical characterization setup. Y. W. performed FDTD simulations. A. M. A. and W. W. aided experimental designs, theoretical analysis, data analysis. All authors have given approval to the final version of the manuscript and Supporting Information.

Notes.

The authors declare no competing financial interest.

ACKNOWLEDGMENTS

This work was supported by Army Research Office (W911NF1810033) and Office of Naval Research (N00014-17-2270). We thank Anna Shaposhnik (USC) for rendering. We thank Rene Zeto (USC) and Ruojiao Sun (USC) for helpful discussions.

REFERENCES

- (1) Guglielmelli, A.; Nemati, S.; Vasdekis, A. E.; Sio, L. D. Stimuli Responsive Diffraction Gratings in Soft-Composite Materials. *J. Phys. D: Appl. Phys.* **2018**, *52* (5), 053001. <https://doi.org/10.1088/1361-6463/aaedf4>.
- (2) Silberstein, E.; Lalanne, P.; Hugonin, J.-P.; Cao, Q. Use of Grating Theories in Integrated Optics. *J. Opt. Soc. Am. A* **2001**, *18* (11), 2865–2875. <https://doi.org/10.1364/JOSAA.18.002865>.
- (3) Cheben, P.; Xu, D.-X.; Janz, S.; Densmore, A. Subwavelength Waveguide Grating for Mode Conversion and Light Coupling in Integrated Optics. *Opt. Express* **2006**, *14* (11), 4695–4702. <https://doi.org/10.1364/OE.14.004695>.
- (4) Rashid, I.; Butt, H.; Yetisen, A. K.; Dlubak, B.; Davies, J. E.; Seneor, P.; Vechhiola, A.; Bouamrane, F.; Xavier, S. Wavelength-Selective Diffraction from Silica Thin-Film Gratings. *ACS Photonics* **2017**, *4* (10), 2402–2409. <https://doi.org/10.1021/acsphotonics.7b00419>.
- (5) Ettabib, M. A.; Liu, Z.; Zervas, M. N.; Wilkinson, J. S. Optimized Design for Grating-Coupled Waveguide-Enhanced Raman Spectroscopy. *Opt. Express* **2020**, *28* (25), 37226–37235. <https://doi.org/10.1364/OE.410602>.
- (6) Zimmer, J.; Wixforth, A.; Karl, H.; Krenner, H. J. Ion Beam Synthesis of Nanothermochromic Diffraction Gratings with Giant Switching Contrast at Telecom Wavelengths. *Appl. Phys. Lett.* **2012**, *100* (23), 231911. <https://doi.org/10.1063/1.4728110>.
- (7) Li, Y.; Mao, H.; Liu, H.; Yao, Y.; Wang, Y.; Song, B.; Chen, Y.; Wu, W. Stereolithography with Variable Resolutions Using Optical Filter with High-Contrast Gratings. *J. Vac. Sci. Technol. B* **2015**, *33* (6), 06F604. <https://doi.org/10.1116/1.4935336>.
- (8) Yao, Y.; Wang, Y.; Liu, H.; Li, Y.; Song, B.; Wu, W. Line Width Tuning and Smoothening for Periodical Grating Fabrication in Nanoimprint Lithography. *Appl. Phys. A* **2015**, *121* (2), 399–403. <https://doi.org/10.1007/s00339-015-9278-x>.
- (9) Niederer, G.; Herzig, H. P.; Shamir, J.; Thiele, H.; Schnieper, M.; Zschokke, C. Tunable, Oblique Incidence Resonant Grating Filter for Telecommunications. *Appl. Opt.* **2004**, *43* (8), 1683–1694. <https://doi.org/10.1364/AO.43.001683>.
- (10) Beaulieu, M. R.; Hendricks, N. R.; Watkins, J. J. Large-Area Printing of Optical Gratings and 3D Photonic Crystals Using Solution-Processable Nanoparticle/Polymer Composites. *ACS Photonics* **2014**, *1* (9), 799–805. <https://doi.org/10.1021/ph500078f>.
- (11) Ahmed, R.; Butt, H. Diffractive Surface Patterns through Single-Shot Nanosecond-Pulsed Laser Ablation. *ACS Photonics* **2019**, *6* (7), 1572–1580. <https://doi.org/10.1021/acsphotonics.9b00087>.
- (12) Gao, X.; Zhen, B.; Soljačić, M.; Chen, H.; Hsu, C. W. Bound States in the Continuum in Fiber Bragg Gratings. *ACS Photonics* **2019**, *6* (11), 2996–3002. <https://doi.org/10.1021/acsphotonics.9b01202>.
- (13) Oh, J. Y.; Rondeau-Gagné, S.; Chiu, Y.-C.; Chortos, A.; Lissel, F.; Wang, G.-J. N.; Schroeder, B. C.; Kurosawa, T.; Lopez, J.; Katsumata, T.; Xu, J.; Zhu, C.; Gu, X.; Bae, W.-G.; Kim, Y.; Jin, L.; Chung, J. W.; Tok, J. B.-H.; Bao, Z. Intrinsically Stretchable and Healable Semiconducting Polymer for Organic Transistors. *Nature* **2016**, *539* (7629), 411–415. <https://doi.org/10.1038/nature20102>.
- (14) Tee, B. C. K.; Ouyang, J. Soft Electronically Functional Polymeric Composite Materials for a Flexible and Stretchable Digital Future. *Adv. Mater.* **2018**, *30* (47), 1802560. <https://doi.org/10.1002/adma.201802560>.
- (15) Kim, K.; Park, Y.-G.; Hyun, B. G.; Choi, M.; Park, J.-U. Recent Advances in Transparent Electronics with Stretchable Forms. *Adv. Mater.* **2019**, *31* (20), 1804690. <https://doi.org/10.1002/adma.201804690>.
- (16) Wang, Y.; Liu, X.; Li, S.; Li, T.; Song, Y.; Li, Z.; Zhang, W.; Sun, J. Transparent, Healable Elastomers with High Mechanical Strength and Elasticity Derived from Hydrogen-Bonded Polymer

Complexes. *ACS Appl. Mater. Interfaces* **2017**, *9* (34), 29120–29129. <https://doi.org/10.1021/acsami.7b08636>.

(17) Geiger, S.; Michon, J.; Liu, S.; Qin, J.; Ni, J.; Hu, J.; Gu, T.; Lu, N. Flexible and Stretchable Photonics: The Next Stretch of Opportunities. *ACS Photonics* **2020**, *7* (10), 2618–2635. <https://doi.org/10.1021/acspophotonics.0c00983>.

(18) Li, L.; Lin, H.; Qiao, S.; Huang, Y.-Z.; Li, J.-Y.; Michon, J.; Gu, T.; Alosno-Ramos, C.; Vivien, L.; Yadav, A.; Richardson, K.; Lu, N.; Hu, J. Monolithically Integrated Stretchable Photonics. *Light Sci. Appl.* **2018**, *7* (2), 17138–17138. <https://doi.org/10.1038/lsa.2017.138>.

(19) Nocentini, S.; Riboli, F.; Burresi, M.; Martella, D.; Parmeggiani, C.; Wiersma, D. S. Three-Dimensional Photonic Circuits in Rigid and Soft Polymers Tunable by Light. *ACS Photonics* **2018**, *5* (8), 3222–3230. <https://doi.org/10.1021/acspophotonics.8b00461>.

(20) Quan, Y.-J.; Kim, Y.-G.; Kim, M.-S.; Min, S.-H.; Ahn, S.-H. Stretchable Biaxial and Shear Strain Sensors Using Diffractive Structural Colors. *ACS Nano* **2020**, *14* (5), 5392–5399. <https://doi.org/10.1021/acsnano.9b08953>.

(21) Peng, W.; Liao, Q.; Song, H. A Nanograting-Based Flexible and Stretchable Waveguide for Tactile Sensing. *Nanoscale Res. Lett.* **2021**, *16* (1), 23. <https://doi.org/10.1186/s11671-021-03488-0>.

(22) Simonov, A. N.; Grabarnik, S.; Vdovin, G. Stretchable Diffraction Gratings for Spectrometry. *Opt. Express* **2007**, *15* (15), 9784–9792. <https://doi.org/10.1364/OE.15.009784>.

(23) Xu, L.; Liu, N.; Ge, J.; Wang, X.; Fok, M. P. Stretchable Fiber-Bragg-Grating-Based Sensor. *Opt. Lett.* **2018**, *43* (11), 2503–2506. <https://doi.org/10.1364/OL.43.002503>.

(24) Yin, K.; Lee, Y.-H.; He, Z.; Wu, S.-T. Stretchable, Flexible, Rollable, and Adherable Polarization Volume Grating Film. *Opt. Express* **2019**, *27* (4), 5814–5823. <https://doi.org/10.1364/OE.27.005814>.

(25) Yu, D.; He, Y.; Liu, H.; Wang, B.; Li, L.; Wang, R.; Luo, S. Characterizing the Bending Deformation of Polymer Utilizing the Diffraction Spectrum of a Holographic Grating on a Flexible Substrate. *Opt. Lett.* **2020**, *45* (2), 579–582. <https://doi.org/10.1364/OL.374653>.

(26) Mahpeykar, S. M.; Xiong, Q.; Wei, J.; Meng, L.; Russell, B. K.; Hermansen, P.; Singhal, A. V.; Wang, X. Stretchable Hexagonal Diffraction Gratings as Optical Diffusers for In Situ Tunable Broadband Photon Management. *Adv. Opt. Mater.* **2016**, *4* (7), 1106–1114. <https://doi.org/10.1002/adom.201600122>.

(27) Ghisleri, C.; Siano, M.; Ravagnan, L.; Potenza, M. A. C.; Milani, P. Nanocomposite-Based Stretchable Optics. *Laser Photonics Rev.* **2013**, *7* (6), 1020–1026. <https://doi.org/10.1002/lpor.201300078>.

(28) Chen, W.; Liu, W.; Jiang, Y.; Zhang, M.; Song, N.; Greybush, N. J.; Guo, J.; Estep, A. K.; Turner, K. T.; Agarwal, R.; Kagan, C. R. Ultrasensitive, Mechanically Responsive Optical Metasurfaces via Strain Amplification. *ACS Nano* **2018**, *12* (11), 10683–10692. <https://doi.org/10.1021/acsnano.8b04889>.

(29) Wang, Y.; Li, T.; Li, S.; Guo, R.; Sun, J. Healable and Optically Transparent Polymeric Films Capable of Being Erased on Demand. *ACS Appl. Mater. Interfaces* **2015**, *7* (24), 13597–13603. <https://doi.org/10.1021/acsami.5b03179>.

Graphical Table of Contents Entry

